FIELD-INDUCED PHASE TRANSITION AND RELAXOR CHARACTER IN SUBMICRON STRUCTURED LEAD-FREE $(Bi_{0.5}Na_{0.5})_{0.94}Ba_{0.06}TiO_3$ PIEZOCERAMICS AT THE MORPHOTROPIC PHASE BOUNDARY

Lorena Pardo[1]*, Elisa Mercadelli[2], Álvaro García[1], Klaus Brebøl[3] and Carmen Galassi[2]

[1] *Instituto de Ciencia de Materiales de Madrid. Consejo Superior de Investigaciones Científicas (ICMM-CSIC). Cantoblanco. 28049- Madrid (Spain)*
[2] *National Research Council, Institute of Science and Technology for Ceramics (CNR-ISTEC). Via Granarolo, 64. I-48018 Faenza (Italy)*
[3]*Limiel ApS. DK-4772 Langebæk. (Denmark)*
**E-mail address: lpardo@icmm.csic.es*

IEEE Transactions on Ultrasonics, Ferroelectrics and Frequency Control
(ISSN: 0885-3010, ESSN: 1525-8955)
Vol. 58 issue 9, pp. 1893-1904 (2011)

Abstract

Submicron-structured $(Bi_{0.5}Na_{0.5})_{0.94}Ba_{0.06}TiO_3$ ceramics (<G> <720nm) from nanopowders were studied. The real part of the optimum room temperature set of piezoelectric coefficients obtained from resonances of the BNBT6 dense ceramic disks and shear plates (d_{31}= (-37+1.33i) $pC.N^{-1}$, d_{15}=(158.3 -8.31i) $pC.N^{-1}$, k_t= 40.4%, k_p=26.8% and k_{15}=40.2%) and d_{33} (148 $pC.N^{-1}$) can be compared with the reported properties for coarse-grained ceramics. Shear resonance of thickness poled plates is observed at T=140ºC. Permittivity vs. temperature curves of poled samples show relaxor character up to T_i=230ºC on heating and T_i=210ºC on cooling of the depoled samples. The phase transition from the room temperature ferroelectric (FE) to a Low Temperature Non-Polar at Zero Field (LTNPZF) phase can be observed as a sharp jump in $\varepsilon^{\sigma}_{33}'(T)$ curves or, as the degree of poling decreases, as a soft change of slope of the curves at $T_{FE\text{-}LTNPZF} = T_d$= 100ºC. This dielectric anomaly is not observed on cooling of depoled samples, as the FE phase is field-induced. The observed macroscopic piezoelectric activity above T_d is a consequence of the coexistence of nanoregions of the FE phase in the interval between $T_{FE\text{-}LTNPZF}$ and T_i.

Introduction

The challenge to develop high piezoelectric sensitivity and lead-free composition ferroelectric ceramics has brought new interest to the study of some classical ferroelectrics as $(Bi_{0.5}Na_{0.5})TiO_3$ (BNT) [1], $BaTiO_3$ (BT) [2] and their solid solutions [3].

The A-site substituted compound BNT was known as ferroelectric shortly before 1961 [1] and presents a sequence of phase transitions, with very large coexistence ranges of the different symmetries of the perovskite-type structure [4,5], which is not unique but it is quite unusual. Early experimental studies on a number of physical properties (dielectric, mechanical, optical, etc.) [4,5] evidenced four peculiar temperatures of BNT, namely: three phase transitions: at 200ºC (from Ferroelectric (FE) to Antiferroelectric (AFE)), at 320ºC (from AFE to Paraelectric (Ferroelastic) (PE(Felast))), at 540ºC (from PE(Felast) to Paraelectric (Paraelastic) (PE(Pelast))); and the point of isotropization of the optical properties. Such a point shows a temperature hysteresis (230ºC on cooling and 280ºC on heating). First structural studies of BNT determined that at room temperature it is rhombohedral (R), *R3c*, above 320ºC it is tetragonal (T), with a non-centrosymmetric and polar space group, *P4mm*, and above 540ºC its prototypic cubic(C), $Pm\bar{3}m$, phase takes place.

Within this structural sequence, in the interval between 200 and 320ºC the correlation between properties and structure was not well understood. The mixture of R and T phases evidenced by X-ray and neutron diffraction studies does not explain the antiferroelectricity (double hysteresis loops) observed in that range. Due to this, the phase in that range of temperature was called instead Low Temperature Non-Polar phase [5] at Zero Field (LTNPZF). Above 450ºC the dielectric curve fulfills the Curie-Weiss law, thus confirming the paraelectric performance in that range of temperature, reason why the space group of the T phase could not be polar.

As a result of this contradictory data, the phase transitions and coexistence ranges of BNT [6-10] and even the room temperature structure [11,12], are under revision. A Transmission Electron Microscopy (TEM) study in a hot-stage [8,9] showed a modulated phase between 200 and 300ºC, formed by orthorhombic *Pnma* sheets progressively appearing within the R phase. The new orthorhombic phase was evidenced as single phase between 280 and 320ºC before a PE(Felast) tetragonal *P4/mbm* one with a centrosymmetric point group. The relaxor character [13] and antiferroelectricity [14] has been explained for BNT in terms of these structural features. The relaxor character is generally attributed to the presence of polar nanoregions (PNRs), characterized by local order.

Though losses and conductivity can be controlled [15], which provides proper poling, BNT ceramics have a piezoelectric coefficient d_{33}=73 $pC.N^{-1}$ that is too low for their practical use [16]. For this, a large number of BNT-based solid-solution systems have been tested to

improve the piezoelectric properties [3]. Solid solutions with Morphotropic Phase Boundary (MPB) are being sought as a starting point for identifying high sensitivity lead-free piezoelectric ceramics [17-20]. In particular, ceramics in the system (1-x) $(Bi_{0.5}Na_{0.5})TiO_3$-$xBaTiO_3$ [21,22] have been studied and it was found that there is a MPB in the Phase Diagram of poled ceramics [23], between R (BNT-like) and T (BT-like) ferroelectric phases at room temperature for compositions close to x=0.06 (BNBT6) [24]. Recent results [25,26] have found that the Phase Diagram of unpoled ceramics differs from the one of poled ceramics, due to the electric-field induced phase transitions observed for BNT-based solid solutions [17,27-32]. Due to this structural peculiarity, the piezoelectric activity of BNBT6 is not as high as expected by similitude to the $PbZrO_3$-$PbTiO_3$ (PZT) system for compositions near the MPB. Nevertheless, since a thickness coupling factor of 55% and a piezoelectric coefficient d_{33}=125 $pC.N^{-1}$ were reported in 1991 [21] for pressure-less sintered ceramics at 1200ºC-2h in air, BNBT6 can be considered a good candidate for lead-free piezoelectric ceramics.

Processing of ceramics from nanopowders allows nowadays getting fine grained, submicron structured, ceramics. These are of interest both for the basic studies of size-effects in ferroelectrics and for their use as high frequency ultrasonic transducers, because they allow the miniaturization of devices. Nanopowders of BNBT6 have been recently obtained by the sol gel auto-combustion method [33]. This synthesis method results in primary particle size of few tenths of nanometers, as well as in stoichiometry and microstructure control by reduction of the processing temperature of piezoceramics when combined hot pressing and recrystallization at moderate higher temperature [34] are used. Some new phenomena, like the microstructural stabilization of ferroelectric phases that enhance piezoelectricity, have recently been reported for submicron and nanostructured lead-free piezoceramics [35, 36]. Nevertheless, little work has been done to date on these, since generally the decrease in grain size reduces the piezoelectricity of ceramics [37, 38].

To gain information on their performance as ultrasonic transducers and understanding of their thermal stability, the study of submicron structured BNBT6 ceramics is here presented. They were prepared from nanometric powder obtained by sol-gel autocombustion synthesis by a combination of hot-pressing and recrystallization. The piezoelectric, elastic and dielectric coefficients at resonance of thin disks and shear plates, both thickness poled, are determined including all losses. The thermal evolution of the dielectric permittivity and shear coupling coefficient of these ceramics were determined. Discussion of these is presented in terms of the crystal structure and ceramic microstructure.

Experimental method

(1-x) $(Bi_{0.5}Na_{0.5})TiO_3$-x$BaTiO_3$ with x=0.06 (BNBT6) nanometric (15-30 nm) powder was synthesized by a citrate nitrate sol gel auto-combustion method, details of which are explained elsewhere [33]. In this process, the pure perovskite phase is directly obtained by heating the gel at 500ºC. Pellets of the powder of 15 mm diameter and 1 mm thickness were obtained by uniaxial pressure forming followed by cold isostatic pressing at 200 MPa. Aiming at reducing the loss of volatiles and keeping submicron grain size and dense microstructure, a combination of hot-pressing at low temperature (700-800ºC for 2h, at 20MPa in air, using heating and cooling rates of 3 ºC.min^{-1}) and subsequent recrystallization [34] at higher temperature (1000 and 1050ºC for 1h in air) has been applied to sintering the green pellets. Ceramics were characterized using X-ray diffraction (XRD) and scanning electron microscopy (FEG-SEM, NOVA NANOSEM 230 with beam deceleration module) and their density was obtained by Archimedes method. Computer assisted quantitative microstructural characterization (MIP45 Digital Image System) was carried out by analysis and measurements on SEM and optical microscopy images (Leitz Laborlux 12 MES/ST). Both mean grain and pore size of the ceramics were determined as the equivalent diameter to a circular shape ($D_{eq}=4(S/\pi)^{1/2}$, where S=grain or pore surface area) and from the analysis of the measured lognormal distributions of equivalent diameter [39].

Sintered disks were ground to a thickness (t) to diameter (D) ratio below 1/20 (typically t=0.7 and D=15mm) and Ag electrodes were attached at their major faces for the electric poling in thickness and for the impedance measurements at the radial and thickness resonance modes. Rectangular plates of a lateral dimensions (L,w) to thickness (t) aspect ratio below 1/10 (typically t=0.5 and L,w=5mm) were also cut from the sintered ceramic disks, electroded and thickness poled. Poling electrodes were mechanically removed and a new pair of electrodes was applied on two of their perpendicular faces for the impedance measurements.

Owing to the reduced d.c. ceramic conductivity, it was possible to carry out poling of disks and plates at T_p=180ºC in a silicone oil bath up to fields of 40-60 kV.cm^{-1}, depending on the slightly variable dielectric strength of the samples. Ceramics were hot-poled for 30 minutes and cooled down to room temperature with the field applied. The d_{33} piezoelectric coefficient was measured in a Berlincourt meter a day after samples poling. Impedance measurements as a function of the temperature were carried out at various frequencies in the range between 1kHz and 1MHz with a HP4194A analyzer. The heating and cooling rates were 2ºC/min. From these experimental data and the geometric factor thickness/area, the complex relative dielectric permittivity, $\varepsilon^* = \varepsilon' - i\varepsilon''$, and dielectric losses, $\tan\delta = \varepsilon''/\varepsilon'$, were obtained.
This experimental set-up was also used for the measurement of electromechanical resonance as a function of the temperature.

Piezoelectric coefficients of ferroelectric ceramics are currently calculated using standard methods [40] from the measurements of complex impedance data on a number of electromechanical resonances and their analysis. The shear coefficients have been scarcely reported in the literature for ceramics of BNT-based compositions [15, 22], though they are needed for the matrix characterization required for 3-D computations by numerical methods [41]. This is due to the complexity of the achievement of the in-plane-poled geometry required for the standard methods of measurement and to produce virtually monomodal resonators. The resonance method is strictly valid just for monomodal resonators. Standards cannot determine all material coefficients in complex form, thus including all types of losses [42]. To overcome the mentioned limitations and difficulties, an alternative method has been developed and will be used in this work for the determination of the material coefficients from thickness-poled and length excited shear plates [41]. Decoupled shear modes of resonance were obtained for samples with aspect ratio (w/t) optimized by fine-tuning of the thickness.

Complex impedance measurements at resonance were carried on using a HP4192A impedance analyzer controlled via a GPIB-PCIIA (National Instruments) interface board. Alemany et al. software was used here for the calculation of the complex piezoelectric, elastic and dielectric coefficients in each mode of resonance, as well as for the determination of the corresponding electromechanical coupling factors and frequency numbers. Details of the calculations are explained elsewhere for the thickness [43] and planar [44] resonance modes of thin disks, poled and excited in thickness, as well as for the shear resonance mode of thickness poled thin plates [41]. After the calculation of the complex parameters, the resonance spectrum is reconstructed as an accuracy test of the final set of calculated coefficients. The accuracy of the material parameters is also quantified by the regression factor (R^2) of such reconstruction to the experimental spectrum. It has to be mentioned that there is a good agreement between the real part of the coefficients calculated by this method and the standard ones. This method also provides the imaginary part of the complex parameters thus giving all the material losses as additional information.

Experimental results

As previously evidenced [34], the ceramics here studied are single phase and have at room temperature a distorted perovskite structure. The crystal structure of unpoled BNBT6 ceramics at the MPB has been controversial until recent studies that clarify the differences between unpoled and poled samples. The MPB structure shows a mixed character due to the coexistence of BNT-like structure (R) and BT-like structure (T) phases [31, 45]. Fig.1(a) and (b) shows selected peaks of the XRD patterns of the room temperature structure of poled ceramics measured after removal of one of the electrodes. The selected º2θ windows show the

splitting of the normalized peaks (006) and (202) (Fig.1(a)), that indicate the presence of the rhombohedral features of the structure (BNT-like), and the splitting of the (002) and (200) peaks (Fig.1(b)), of the tetragonal features of the structure (BT-like). Such a clear splitting and peak intensity ratios are not observed in unpoled ceramics [31, 34], being the higher the relative height of the (006)-R (Fig.1(a)) and (002)-T (Fig.1(b)) peaks, the higher the polarization level of the ceramic.

Fig. 2 shows the SEM images of the ceramics. Table 1 summarizes the relative density, the parameters from the quantitative characterization of grain and pore size, as well as the total porosity, and the material data (e_{15}, d_{15}, h_{15}, g_{15}, s_{55}^{E}, ε^{S}_{11}, $\varepsilon^{\sigma}_{11}$, k_{15}, N_{15}) obtained from the shear resonance of thickness poled plates of optimum aspect ratio of the BNBT6-1 to 3 samples. Similarly, Table 2 summarizes piezoelectric (d_{33}, h_{33}, e_{33}, d_{31}, g_{31}), elastic (c_{33}^{D}, s_{11}^{E}, s_{12}^{E}, s_{66}^{E}) and dielectric (ε^{S}_{33}, $\varepsilon^{\sigma}_{33}$) linear coefficients, including all losses, measured at the planar and thickness resonances of thin disks for the same ceramics. The Poisson ratio, electromechanical coupling factors (k_p, k_t) and frequency numbers (N_p, N_t) are shown in Table 2. Tables 1 and 2 show also published data for air-sintered BNBT6 ceramics obtained by mixed oxides method [21,22, 45] and with BNT ceramics [15] for the sake of comparation.

Fig. 3 shows the resonance spectra (R and G peaks) of the planar (Fig. 2(a)) and thickness (Fig. 2(b)) modes of a thin disk and the shear mode of a, thickness-poled and length excited, shear plate (coupled (Fig. 2(c)) and decoupled (Fig. 2(d)) by fine-tuning of the thickness) of BNBT6-3 ceramic. These spectra are shown here to assess the accuracy of the parameters in Tables 1 and 2. Both the experimental (symbols) and reconstructed spectra (lines) are shown for each spectrum together with the regression factor of the latter to the experimental ones. It is noticeable the difference of R^2, which is a quantitative evaluation of the accuracy of the calculation, from the coupled and decoupled shear resonance mode of the plate. This arises from the fact that coupled modes cannot be reproduced (low R^2) with a single mode model, as the one used here [41]. Decoupled modes are used for the calculation of the parameters in Table 1.

Fig.4 and 5 shows the real part of the relative dielectric permittivity and the dielectric loss as a function of the temperature for the BNBT6-1 to 3 samples. Fig. 4 shows results in poled ceramics, measured on heating. Fig.5 shows the same information for the thermally depoled ceramics, measured on cooling. The differences between heating and cooling measurements will be discussed in the following in terms of the field-induced phase transition.

Fig.6 shows the impedance spectrum of the shear mode of resonance at 140ºC during the thermal depolarization process of a BNBT-3 plate. This result is in contrast with the reported vanishing of the radial mode of thin disks of BNBT6 [46] and with the vanishing of the thickness mode of the the BNBT-3 disk, both at $T \approx 100$ºC, also shown in Fig. 6.

Discussion

I. Electromechanical properties: room temperature values and thermal evolution.

In a previous work [34], it was proved the principle of enhancing the piezoelectric performance of BNBT6 ceramics hot-pressed at low temperature (700ºC-800ºC for 2h) by recrystallization at a moderately higher temperature (1000ºC). However, the best combination of the hot pressing and recrystallization temperatures to get optimum properties was not determined. Here (Tables 1 and 2) we show that the optimum set of room temperature piezoelectric coefficients is that of the BNBT6-3 dense (95.4% of the theoretical density for the nominal composition, 5.9245 $g.cm^{-3}$)) and submicron structured (<G >=680 nm) sample (d_{33}=148 $pC.N^{-1}$, d_{31}= (- 37+1.33i) $pC.N^{-1}$, d_{15}=(158.3 -8.31i) $pC.N^{-1}$, k_t= 40.4%, k_p=26.8% and k_{15}=40.2%). The real values of the properties of the dense BNBT6-3 sample compare well with those reported for coarse-grained ceramics prepared at higher sintering temperatures, despite of their submicron structure and previous trends found in the literature [37,38].

As previously evidenced [34], this set of interesting properties is due to a controlled microstructure and stoichiometry of these ceramics, resulting from the processing route used, with respect to those reported previously and obtained with processing temperatures higher than 1100ºC. Such a characteristics of the ceramics here studied allows poling at T_p=180ºC, temperature higher than those reported, resulting in higher efficiency.

The small differences observed for BNBT6-2 and 3 properties are showing the small differences in grain size, larger for BNBT6-3, and porosity, lower for BNBT6-3, between these two samples (Table 1). For BNBT6-1 the small coefficients obtained are the expected result of a combination of the residual porosity and very fine grain size (Table 1).

For compositions at the MPB of all BNT-based solid solutions, the relatively low thermal stability is considered a drawback for practical applications. Their depolarization temperature T_d up to which macroscopic piezoelectric properties are observed was determined by thermal depolarization currents [45] and resonance measurements as a function of the temperature [15, 17, 18, 46]. T_d for the MPB composition of BNT-based solid solutions is low, T_d ~100ºC. $T_{d,}$ a technologically interesting parameter for these ceramics, has been defined by some authors [15, 17] as the temperature for which the phase of the impedance at resonance becomes zero. It has been repeatedly found that for poled ceramics at T_d there is a sharp jump in the real part of the dielectric permittivity of poled ceramics [3, 15, 17, 18, 19, 38] and a sharp peak in the dielectric losses. Weak electromechanical planar resonance was observed for temperatures higher than T_d [17], which was understood as a result of the coexistence of the room temperature FE and the AFE phases. Fig.6 shows that shear resonance for BNBT6-3

ceramics measured in the depoling process can be clearly observed at 140ºC. T_d is considered as an indication of the stability of the ferroelectric domains. Less stable domains are easy to switch, thus piezoelectric properties (d_{33}) are enhanced for less stable ferroelectric domains that coincides with low depolarization temperature in BNBT compositions [45, 46, 47]. Nevertheless, we found in the ceramics under study evidence of remnant shear resonance well above the reported T_d for BNBT6 and our T_d from measurements of the thickness mode of thin disks (Fig. 6). The depolarization process of BNBT6 is not fully explained and its understanding needs of a better knowledge of the phase transitions involving changes of crystal symmetry in BNT-based solid solutions at the MPB, unusual as those of the end member BNT.

II. Dielectric permittivity as a function of the temperature

Until very recently, the lack of structural information on the BNBT6 composition as a function of the temperature limited the discussion of the thermal evolution of its properties that could only be made by similitude with BNT ceramics and based on the still incomplete information about the peculiar crystal structure of this parent composition. Recently published data on TEM [25], synchrotron XRD [26] and Raman spectroscopy [47] studies for BNBT100x compositions near the MPB allows today a better understanding of the BNBT6 dielectric performance and phase transitions.

(a) Heating of poled samples

The thermal evolution of the real part of the free dielectric permittivity in the poling direction ($\varepsilon^{\sigma}_{33}{}'$) on heating of the poled samples (Fig. 4) shows broad maxima of $\varepsilon_{33}{}^{\sigma\prime}$ at T_m~ 300ºC, a dispersive region that extends up to ~230ºC. A low temperature anomaly can also be observed as a sharp jump for BNBT6-3 and as a soft change of slope of the $\varepsilon_{33}{}^{\sigma\prime}(T)$ curve for BNBT6-1 and 2 at ~ 100ºC

Changes in the maximum value of $\varepsilon^{\sigma}_{33}{}'(T)$ correspond well with changes in the residual porosity (Table 1) of the BNBT6-1 to 3 samples, increasing as density increases in BNBT6-1 to 3. The maxima of $\varepsilon^{\sigma}_{33}{}'(T)$ are frequency dependent, except for BNBT6-3, but T_m takes place at the same temperature for all frequencies. Only the $\varepsilon^{\sigma}_{33}{}'(T)$ curve for the BNBT6-1 sample shows a fast increase (Fig. 4(a)) at low frequency above the T_m, which is reversible as the corresponding curve on cooling (Fig. 5(a)) shows. This is accompanied by high dielectric losses taking place from lower temperatures at lower frequencies (Fig. 4(a)). This phenomenon is due to conductivity and it is frequently found in the literature, commonly starting from lower temperatures for ceramics sintered at T> 1100ºC. It is due to high temperature charge-migration polarization related with crystal defects caused by the loss of volatiles during ceramic processing. This thermal evolution is found in BNT [15] and a number of BNT-based ceramics as well (BNT-$(K,Na)NbO_3$ [18], BNBT6 [48], BNT-$(Bi_{0.5}K_{0.5})TiO_3$-$BaTiO_3$ (BNT-BKT-BT)

[49], BNT-Ba($Al_{0.5}Nb_{0.5}$)O_3 [50]). The reduced conductivity observed above T_m in the dense ceramics studied here, BNBT6-2 and 3, results from their good stoichiometry [34], derived from the low processing temperatures (1000-1050ºC) with respect to the currently reported ones, which prevent Bi losses.

$\varepsilon^{\sigma}_{33}'$(T) curves are highly dispersive up to ~230ºC on heating (Fig. 4). This upper limit temperature for the dispersive region is often ascribed in BNT-based compositions [15,17, 18] to T_{R-T}, the transition temperature from the room temperature R(FE) to the T(AFE) phase by similitude with BNT. However, it resembles more to the isotropization point (T_i) of the optical properties in BNT, which is also associated to a local maximum in the first derivative of the real part of the dielectric permittivity vs. temperature curve dε′/dT [4, 5]. According to recent structural data for BNT [9] the isotropization point (280ºC) can be ascribed to the upper limit of occurrence of the modulated phase before transition to the orthorhombic phase when heating. Early interpretation [4] of T_i on cooling involved the percolation phenomena of the AFE regions that begin to form at T_m within the Felast twins formed in the PE(Felast) phase, which in turn originates at 540ºC on cooling from the PE(Pelast) cubic phase. This percolation creates long-range AFE order in the crystal. On heating, the complete separation of AFE regions can only take place when a critical density of P(Felast) interlayer takes place. This requires a higher temperature, thus the observed thermal hysteresis of T_i. It is clear that the temperature of formation on cooling and destruction on heating of the long range ordered AFE phase will correspond to the most unstable state of the crystal and thus to a dε′/dT local maximum. Obviously experimental data on BNBT6 structure is needed to clarify the nature of such an AFE (more properly LTNPZF) phase. Recent TEM work on unpoled ceramics [25] suggests that the LTNPZF phase is constituted by AFE nanoregions in a non-polar phase. Authors of such a work coined the term antiferroelectric-relaxor for this phase. It seems clear that T_i differs from the lower limit of occurrence of the LTNPZF phase on heating from the room temperature FE phase, $T_{FE-LTNPZF}$ (or T_{R-T} for similitude with BNT).

In the dispersive region (T<230ºC) the low temperature anomaly can be observed, as a sharp jump at ~ 100ºC for BNBT6-3 and as a change of slope of the $\varepsilon^{\sigma}_{33}'$(T) curves for BNBT6-1 and 2. In our results (Fig. 4), $T_{FE-LTNPZF}$ is indicated by this anomaly. The sharp jump at 100ºC in the $\varepsilon^{\sigma}_{33}'$(T) curve of poled BNBT6-3 ceramics has also been observed by other authors in BNBT6 coarse grain poled ceramics [19, 38,47,51,52] and, at other temperatures, in poled BNT [15] and in BNT- or BKT-based solid solution ceramics [3,17,18] and it is currently ascribed to the depolarization temperature (T_d). For PZT and most of the classical piezoceramics the depolarization temperature, which establishes the disappearance of the long-range order polarization and related properties, is ascribed to the transition temperature between the FE phase and the paraelectric (or High Temperature Non Polar (HTNP)) one. For $NaNbO_3$

coarse grain ceramics depolarization takes place at the transition from a field-induced FE phase to an intermediate AFE phase, before the paraelectric one [36], which resembles more the situation found here.

For ceramics BNBT6-2 on heating of the poled samples, the losses present three characteristic features (Fig. 4(b)) as the temperature increases, namely, a sharp decrease of the losses and two broad and frequency dependent peaks of these. The highest temperature feature, observed as well for unpoled ceramics (Fig. 5(b)) at 340ºC at 1KHz and above 450ºC at 1 MHz, is a broad peak characteristic of a relaxation. This could be related with the reported structural transition from the T (PE(Felast)) to the C (PE(Pelast)) phases observed at 540ºC for BNT [4]. This is also reflected sometimes in the $\varepsilon^{\sigma}_{33}{}'(T)$ curve as a slight change in the slope of the curve at ~ 400ºC (Fig. 4 (b) and (c)). At intermediate temperatures, there is a second maximum in the losses that appears at ~240ºC at 1 kHz and at ~330ºC at 1MHz. This could be related with the dispersion of $\varepsilon_{33}{}^{\sigma}{}'$ at the maximum (T_m ~ 300ºC) (Fig. 4(b)) since these maxima are not observed for the depoled samples. The thermal evolution of the losses at 1 MHz is consistent with the observed one for ceramics of BNT-BKT-BT composition at the BNT-like structure (R) side of the MPB [17]. The characteristic feature at lower temperature is the decrease of the losses from a frequency dependent temperature above ~140ºC for all ceramics. The change as a function of the frequency of the shoulder of $\varepsilon^{\sigma}_{33}{}'(T)$ in the dispersive region and this low temperature anomaly in the losses (Fig. 4(b)) are characteristic of the relaxor character.

For BNBT6-1 the conductivity, most probably related with the high density of grain boundary and porosity, produces an increase in the a.c. losses (Fig. 3(a)) and masks all other features of the tanδ(T) curves above the low temperature anomaly. For this sample, the intermediate anomaly can only be seen at 330ºC in the curve measured at 1 MHz.

For BNBT6-3 there is a minor peak superimposed to this low temperature broad anomaly in tanδ (Fig. 3(c)) at the same temperature (T~100ºC) of the sharp jump in the $\varepsilon^{\sigma}_{33}{}'(T)$ curve. This low temperature feature, though as a wide sharp peak, has also been observed in coarse grain BTN and BNT-based ceramics in coincidence with the temperature of the sharp anomaly in the $\varepsilon^{\sigma}_{33}{}'(T)$ curve for poled samples. For the submicron-structured ceramics studied, for which the FE-LTNPZF transition extends over a wider temperature range, this peak of the losses at T_d seems to be masked by the relaxor performance.

(b) Cooling of thermally depoled samples

The main features of the real part of the dielectric permittivity measured on cooling for the depoled samples (Fig. 5) are the wide maximum, as observed on heating but with a slightly lower T_m, and a dispersive region, for T<210ºC. As for the thermal hysteresis concerning the

upper limit of the relaxor region, the isotropization point as in BNT, it was indeed found at a higher temperature (230ºC) on heating (Fig. 4).

These features were also observed previously for unpoled ceramics of similar composition near the MPB (BNBT6 [15, 53], BNBT5.5 [54] and BNBT7 ceramics [55]), as well as BNBT6 single-crystals [56]. The freezing temperature of the PNRs causing this relaxor performance was determined as ~ - 10ºC in BNBT5.5 unpoled ceramics [54] and, therefore, they cannot be disregarded at room temperature. In fact, synchrotron x-ray diffuse scattering studies [11] and TEM studies [14] have provided evidence of tetragonal (AFE) inclusions at the nanoscale in the room temperature phase of ceramics of the parent BNT composition. According to recent TEM studies [25] the room temperature phase of unpoled BNBT6 is an antiferroelectric relaxor, inhomogeneous at the nanoscale.

These features of the ε´(T) curves are accompanied by two anomalies in the losses. At low temperature (Fig. 5), a decrease of the losses takes place from a temperature in an interval of ~ 100ºC at 1kHz to ~140ºC at 1MHz. At high temperature, a relaxation with a maxima taking place from 350ºC at 1KHz up to above 450ºC at 1 MHz can be observed. These maxima are masked by losses above 350ºC in BNBT6-1 and 2.

As reported before, on cooling the depoled samples there is no sign of the dielectric anomaly that should appear at $T_{FE\text{-}LTNPZF}$. This anomaly can be observed again on heating only when repoling the samples. The LTNPZF phase in BNBT6 ceramics was evidenced by pinched loops at 130ºC [47 51] or even at room temperature [48]. Our results on ε´(T) curves are also in agreement with recent Raman spectroscopy data on unpoled BNBT6 ceramics as a function of the temperature [47] that did not show evidence of local structure change for the expected phase transition at $T_{FE\text{-}LTNPZF}$.

Recently, electric-field-induced changes of the crystal structure in BNT-based poled samples with respect to the unpoled state have been reported [17,27,28,29,30,31]. The pseudocubic structure observed in submicron structured unpoled BNBT6 ceramics [34] is contradictory with the fact that the poled ceramics are FE and have noticeable piezoelectric properties (Tables 1 and 2). The long-range order characteristic of the FE phase cannot be developed in relaxors under natural conditions. The application of an electric field is necessary to create a FE phase from a relaxor. The lack of the frequency dispersion in a dielectric curve is related to the appearance of long-range order in a FE phase. Figs. 1(a) and (b) shows that poled ceramics have a dominant rhombohedral structure, with a higher intensity ratio of the (006) to the (202) peak as porosity decreases, that accounts with the macroscopic properties and reveals the structural transition induced by the electric field. Though some degree of relaxor character is observed even at room temperature for poled ceramics, these have a lower dispersion (Fig.4) than the depoled ones (Fig.5). The dielectric dispersion and hysteresis here found (Figs. 4 and

5) also indicate that the poling treatment gives place to a field-induced FE phase via a structural transition and, therefore, it cannot be observed when cooling the depoled samples.

The poling efficiency for all ceramics studied most probably results from poling above $T_{FE\text{-}LTNPZF}$. The mechanisms underlying this result are still unclear, but they are most probably related with the possibility of easier field-induced structural transitions to a FE phase in the matrix phase around the AFE PNRs and also in these PNRs when $T_{FE\text{-}LTNPZF} < T_p < Ti$.

Domain walls act as nucleation sites for electric-field-induced structural transitions that take place at lower fields in multidomain state, which is the reason underlying the observations of enhancement of piezoelectric coefficients when domain size is reduced [57]. We may use here these principles of domain engineering in single-crystals to explain the poling efficiency in our ceramics. Grain size reduction of ceramics reduces domain size, thus increasing the domain wall density, and hence the observation of piezoelectric coefficients comparable to coarse-grained materials instead of the expected reduction of these.

For application point of view, our results indicate that the depolarization process on these ceramics must not only be regarded as a process of domain dynamics up to $T_{FE\text{-}LTNPZF}$, but it must also be related with temperature driven local structural changes in the temperature region of stability of the relaxor LTNPZF phase. The macroscopic electromechanical activity also indicates coexistence of field-induced FE phase above $T_{FE\text{-}LTNPZF}$, giving place to non-negligible macroscopic polarization for temperatures much higher than the reported $T_d=T_{FE\text{-}LTNPZF}$ ~100ºC. These experimental results of the authors (Fig.6) will be reported in detail separately.

Conclusions

Submicron structured (<G><720 nm), dense BNBT6 ceramics obtained from sol-gel combustion nanopowders by a combination of hot-pressing (700-800ºC) and recrystallization at moderate temperature (1000 or 1050ºC) were studied. The $\varepsilon^{\sigma}_{33}{}'(T)$ curves on heating of the poled samples show a diffuse transition at $T_{FE\text{-}LTNPZF}$ ~100ºC or a sharp jump at the same temperature as the porosity decreases and the polarization degree increases. The $\varepsilon'(T)$ curves on cooling of the thermally depoled samples do not show the expected anomaly at $T_{FE\text{-}LTNPZF}$. This and the XRD results on poled samples indicate that the poling field induces the FE phase. Poled or thermally depoled samples show a relaxor region extending to room temperature below a threshold temperature, whose thermal hysteresis (230ºC on heating and 210ºC on cooling) resembles that of the isotropization point of the optical properties of the parent BNT composition. The diffuse transition FE-LTNPZF most probably indicates that the FE phase coexists at the nanoscale in the temperature range of the occurrence of the LTNPZF one. This is in agreement with the non-negligible shear resonance measured at T=140ºC. The BNBT6-3

ceramics with optimized microstructure have room temperature piezoelectric coefficients (d_{33}=148 pC.N^{-1}, d_{31}= (- 37+1.33i) pC.N^{-1}, d_{15}=(158.3 -8.31i) pC.N^{-1}, k_t= 40.4%, k_p=26.8% and k_{15}=40.2%) comparable with those reported previously in coarse-grained ceramics processed at higher temperatures. This is due to the relatively low processing temperatures reducing loss of volatiles and leading to a better controlled stoichiometry and, consequently, to a reduced conductivity that allowed high temperature poling at T_p=180ºC in the region of stability of the relaxor LTNPZF phase.

Acknowledgements

This work was funded by Spanish CSIC project #201060E069 and European Network of Excellence (NoE-MIND CE FP6 515757-2), that established the European Institute of Piezoelectric Materials and Devices (Piezoinstitute). Authors wish to thank Mr. José Luis Millán (FINNOVA 2010 grantee) for his technical assistance in the quantitative microstructural characterization.

References

[1] G.A.Smolenskii, V.A. Isupov, A.I. Agranovskaya and N.N. Krainik. ”New Ferroelectrics of Complex Composition IV”. *Soviet Physics Solid State* 2 (11), 2651- 2654 (1961).
[2] A. von Hippel. “Ferroelectricity, Domain Structure, and Phase Transitions of Barium Titanate”. *Rev. Mod. Phys*. 22 (3), 221-237 (1950).
[3] T.Takenaka, H. Nagata and Y. Hiruma.“Phase Transition Temperatures and Piezoelectric Properties of $(Bi_{1/2}Na_{1/2})TiO_3$- and $(Bi_{1/2}K_{1/2})TiO_3$-Based Bismuth Perovskite Lead-Free Ferroelectric Ceramics”. *IEEE Trans. Ultrasonics, Ferroelectrics and Frequency Control* 56(8), 1595-1612(2009).
[4] I.P. Pronin, P.P. Syrnikov, V.A. Isupov, V.M. Egorov, N.V. Zaitseva. “Peculiarities of Phase transitions in sodium-bismuth titanate”. *Ferroelectrics* 25 , 395-397 (1980).
[5] S. B. Vakhrushev, V.A. Isupov, B.E. Kvyatkovsky, N.M. Okuneva, I.P. Pronin, G.A. Smolensky and P.P. Syrnikov. “Phase transitions and soft modes in sodium bismuth titanate”. *Ferroelectrics* 63, 153-160 (1985).
[6] G.O Jones and P.A.Thomas. “The tetragonal phase of $Na_{0.5}Bi_{0.5}TiO_3$ – a new variant of the perovskite structure”. *Acta Crystallographica B* 56 , 426-430 (2000).
[7] G.O Jones and P.A.Thomas. “Investigation of the structure and phase transitions in the novel A-site substituted distorted perovskite compound $Na_{0.5}Bi_{0.5}TiO_3$”. *Acta Crystallographica B* 58 ,168-178 (2002).
[8] V. Dorcet, G.Trolliard and P.Boullay. “Reinvestigation of Phase Transition in $Na_{0.5}Bi_{0.5}TiO_3$ by TEM. Part I: First Order Rhombohedral to Orthorhombic Phase Transition”. *Chem. Mater.* 20, 5061-5073 (2008).
[9] G.Trolliard and V. Dorcet. “Reinvestigation of Phase Transition in $Na_{0.5}Bi_{0.5}TiO_3$ by TEM. Part II: Second Order Orthorhombic to Tetragonal Phase Transition”. *Chem. Mater.* 20, 5074-5082 (2008).
[10] C.S. Tu, S.H. Huang, C.S. Ku, H.Y. Lee, R.R. Chien, V.H. Schmidt and H. Luo. “Phase coexistence and Mn-doping effect in lead-free ferroelectric $Bi_{1/2}Na_{1/2}TiO_3$ crystals”. *Appl. Phys. Lett*. 96, 062903 (2010).
[11] P.A. Thomas, S. Trujillo, M. Boudard, S. Gorfman and J. Kreisel. “Diffuse X-ray scattering in the lead-free piezoelctric crystals $Na_{1/2}Bi_{1/2}TiO_3$ and Ba-doped $Na_{1/2}Bi_{1/2}TiO_3$”. *Solid State Sciences* 12 , 311-317 (2010).
[12] S. Gorfman and P. A. Thomas. “Evidence for a non-rhombohedral average structure in the lead-free piezoelectric material $Na_{0.5}Bi_{0.5}TiO_3$”. *J. Appl. Cryst.* 43, 1409–1414 (2010).
[13] V. Dorcet and G. Troillard. “A transmission electron microscopy study of the A-site disordered perovskite $Na_{0.5}Bi_{0.5}TiO_3$” *Acta Mater.* 56 , 1753-1761(2008).
[14] V. Dorcet, G.Trolliard and P.Boullay.“The structural origin of the antiferroelectric properties and relaxor behavior of $Na_{0.5}Bi_{0.5}TiO_3$”. *J.Magn.Magn.Mat.* 321 , 1758–1761 (2009).
[15] Y. Hiruma, H. Nagata and T. Takenaka. “Thermal depoling process and piezoelectric properties of bismuth sodium titanate ceramics”. *J.Appl.Phys.* 105 , 084112-1-8 (2009).
[16] J. Rodel, W. Jo, K.T.P. Seifert, E.M. Anton,T. Granzow and D. Damjanovic. “Perspective on the development of lead-free piezoceramics”. *J. Am. Ceram. Soc*. 92 , 1153-1177 (2009).
[17] Y. Hiruma, H. Nagata and T. Takenaka. “Phase Transition Temperatures and Piezoelectric Properties of $(Bi_{1/2}Na_{1/2})$ TiO_3-$(Bi_{1/2}K_{1/2})$ TiO_3-Ba_x TiO_3 LeadFree Piezoelectric Ceramics”. *Jap.J.Appl.Phys.* 45(9B), 7409-7412 (2006).
[18] Y. Hiruma, H. Nagata and T. Takenaka. “Phase diagrams and electrical properties of $(Bi_{1/2}Na_{1/2})TiO_3$-based solid solutions”. *J.Appl.Phys*. 104 ,124106-1-7 (2008).
[19] F. Cordero, F. Craciun, F. Trequattrini, E. Mercadelli, and C. Galassi. "Phase transitions and phase diagram of the ferroelectric perovskite $(Na_{0.5}Bi_{0.5})_{1-x}Ba_xTiO_3$ by anelastic and dielectric measurements" *Phys.Rev. B* 81, 144124-1-10 (2010).
[20] D. Damjanovic. “A Morphotropic Phase Boundary System based on Polarization Rotation and Polarization Extension”. *Appl. Phys. Lett.* 97 , 062906-1-3 (2010).

[21] T. Takenaka, K.Maruyama and K. Sakata. "$(Bi_{1/2}Na_{1/2})TiO_3$-$BaTiO_3$ system for lead-free piezoelectric ceramics". *Jap. J. Appl. Phys.* 30(9B), 2236-2239 (1991).
[22] T. Takenaka, A. Huzumi, T. Hata and K. Sakata. "Mechanical properties of $(Bi_{1/2}Na_{1/2})TiO_3$-based piezoelectric ceramics". *Silicates Industriels* 7(8), 136-142 (1993).
[23] H. Yilmaz, G.L. Messing and S. Trolier-McKinstry. "(Reactive) Templated Grain Growth of Textured Sodium Bismuth Titanate ($Na_{1/2}Bi_{1/2}TiO_3$-$BaTiO_3$) Ceramics—I Processing". *J. Electroceram*. 11(3), 207-215 (2003).
[24] D. Rout, K.S. Moon, V.S. Rao and S.J.L. Kang. "Study of the morphotropic phase boundary in the lead-free $Na_{1/2}Bi_{1/2}TiO_3$-$BaTiO_3$ system by Raman spectroscopy". *J. Ceram. Soc. Japan.* 117(7), 797-800 (2009).
[25] C. Ma, X. Tan, E. Dul´kin and M. Roth. "Domain structure-dielectric property relationship in lead-free (1-x)$(Bi_{1/2}\ Na_{1/2})TiO_3$- x$BaTiO_3$ ceramics". *J.Appl.Phys*. 108, 104105 (2010).
[26] W.Jo, J.E. Daniels, J.L.Jones, X.Tan, P. Thomas, D. Damjanovic and J. Rodel. "Evolving morphotropic phase boundary in lead-free $(Bi_{1/2}\ Na_{1/2})TiO_3$- $BaTiO_3$ piezoceramics". *J.Appl.Phys.* 109, 014110 (2011).
[27] J.E. Daniels, W. Jo, J. Rodel and J.L. Jones."Electric-field-induced phase transformation at a lead-free morphotropic phase boundary: Case study in 93%$(Bi_{0.5}Na_{0.5})TiO_3$-7% $BaTiO_3$ piezoelectric ceramic". *Appl. Phys.Lett.* 95 , 032904-1-3 (2009).
[28] W. Jo, T. Granzow, E. Aulbach, J. Rodel and D. Damjanovic. "Origen of the large strain response in $(K_{0.5}Na_{0.5})NbO_3$-modified $(Bi_{0.5}Na_{0.5})TiO_3$-$BaTiO_3$ lead-free piezoceramics". *J.Appl.Phys.* 105, 094102-1-5 (2009).
[29] J.E. Daniels, W. Jo, J. Rodel, V. Honkimaki and J.L. Jones."Electric-field-induced phase change behaviour in $(Bi_{0.5}Na_{0.5})TiO_3$-$BaTiO_3$-$(K_{0.5}Na_{0.5})NbO_3$: A combinatorial investigation". *Acta Mater.* 58 , 2103-2111 (2010).
[30] J. Kling, X. Tan, W. Jo, H.J. Kleebe, H. Fuess and J. Rodel. "In Situ Transmission Electron Microscopy of Electric Field-Triggered Reversible Domain Formation in Bi-Based Lead-Free Piezoceramics". *J. Am. Ceram. Soc.* 93 (9), 2452–2455 (2010).
[31] G. Pitch, J. Topfer and E. Hennig. "Structural properties of $(Bi_{0.5}Na_{0.5})_{1-x}Ba_xTiO_3$ lead-free piezoelectric ceramics". *J.Eur.Ceram.Soc*. 30, 3445-3453 (2010).
[32] A. J. Royles, A. J. Bell, A. P. Jephcoat, A.K. Kleppe, S.J. Milne and T.P. Comyn. "Electric-field-induced phase switching in the lead-free piezoelectric potassium sodium bismuth titanate". *Appl.Phys.Lett.* 97, 132909 (2010).
[33] E. Mercadelli, C. Galassi, A.L. Costa, S.Albonetti and A. Sanson. "Sol-gel combustion synthesis of BNBT powders" *J. Sol-Gel Sci. and Tech.* 46(1), 39-45 (2008).
[34] L. Pardo, E. Mercadelli, K. Brebøl, A. García and C. Galassi. "Piezoelectric properties of lead-free submicron structured $(Bi_{0.5}Na_{0.5})_{0.94}Ba_{0.06}TiO_3$ ceramics". *Smart Materials and Structures* 19(11), 115007-1-10 (2010).
[35] C. Pithan, Y. Shiratori, A. Magrez, S.B. Mi, J. Dornseiffer and R. Waser. "Consolidation, Microstructure and crystallography of dense $NaNbO_3$ ceramics with ultra-fine grain size". *J. Ceram. Soc. Jap.* 114(11), 995-1000 (2006).
[36] A. Moure, T.Hungría, A.Castro and L. Pardo. "Microstructural effects on the phase transitions and the thermal evolution of elastic and piezoelectric properties in highly dense, submicron structured $NaNbO_3$ ceramics". *J. Mater. Sci.* 45 , 1211-1219 (2010).
[37] A. Herabut and A. Safari. "Processing and Electromechanical Properties of $(Bi_{0.5}Na_{0.5})(1-1.5x)La_xTiO_3$ Ceramics" *J. Am. Ceram. Soc.* 80 [11], 2954-2958(1997).
[38] L. Liu and H.Fan. "Influence of sintering temperatures on the electrical property of bismuth sodium titanate based piezoelectric ceramics". *J Electroceram*. 16 , 293–296 (2006).
[39] J. Ricote and L. Pardo. "Microstructure-properties relationships in Sm-modified lead titanate piezoceramics. Part I: Quantitative study of the microstructure". *Acta Mater.* 44, 1155-1167 (1996).
[40] "IEEE Standard on piezoelectricity". ANSI/IEEE Std. 176-1987. "Piezoelectric properties of ceramic materials and components. Part 2: methods of measurement – Low power". European Standard CENELEC, EN 50324-2 (2002).

[41] L. Pardo, A. Garcia, F. Montero De Espinosa and K. Brebøl. "Shear Resonance Mode Decoupling to Determine the Characteristic Matrix of Piezoceramics for 3-D Modelling". *IEEE Trans. Ultrasonics, Ferroelectrics and Frequency Control* 58 (3), 646-657 (2011).
[42] K.W. Kwok, H.L.W. Chan and C.L. Choy. "Evaluation of the Material Parameters of Piezoelectric Materials by various methods". *IEEE Trans. on Ultrasonics, Ferroelectrics and Frequency Control* 44(4), 733-742 (1997).
[43] Alemany C, Pardo L, Jiménez B, Carmona F,Mendiola J and González AM "Automatic iterative evaluation of complex material constants in piezoelectric ceramics" *J. Phys. D: Appl. Phys.* 27 , 148-155 (1994).
[44] C. Alemany, A. M. Gónzalez, L. Pardo, B. Jiménez, F. Carmona, J. Mendiola "Automatic determination of complex constants of piezoelectric lossy materials in the radial mode" *J. Phys. D: Appl. Phys.* 28 , 945-956 (1995).
[45] B.J. Chu, D.R. Chen, G.R. Li and Q.R. Yin. "Electrical properties of $Na_{1/2}Bi_{1/2}TiO_3$–$BaTiO_3$ ceramics". *J. Eur.Ceram.Soc*. 22 , 2115–2121 (2002).
[46] D.Q. Xiao, L. Wu, J.G. Zhu. "Temperature stability of Lead-free Piezoelectric Ceramics of Perovskite $Bi_{0.5}Na_{0.5}TiO_3$ and $K_{0.5}Na_{0.5}NbO_3$ Families". 18th IEEE International Symposium on the Applications of Ferroelectrics (ISAF2009) 3-27 Aug. 2009. Xiam, P.R. China. DOI:10.1109/ISAF.2009.5307596
[47] B.W. van Eerd, D. Damjanovic, N. Klein, N. Setter and J. Trodahl. "Structural complexity of $(Na_{0.5}Bi_{0.5})TiO_3$ - $BaTiO_3$ as revealed by Raman Spectroscopy". *Phys.Rev.B* 82, 104112-1-7 (2010).
[48] T. Oh and M.H.Kim."Phase relation and dielectric properties in $(Bi_{1/2}Na_{1/2})_{1-x}Ba_xTiO_3$ lead-free ceramics". *Mater.Sci.Eng. B –Solid State Mater.Adv.Technol.*132 , 239–246 (2006).
[49] Y.Li, W. Chen, Q. Xu, J. Zhou, X. Gu, S. Fang. "Electromechanical and dielectric properties of $Na_{0.5}Bi_{0.5}TiO_3$–$K_{0.5}Bi_{0.5}TiO_3$–$BaTiO_3$ lead-free ceramics". *Mat.Chem.Phys.*94 , 328–332 (2005).
[50] Y. Hiruma, H. Nagata and T. Takenaka."Formation of Morphotropic Phase Boundary and Electrical Properties of $(Bi_{1/2}Na_{1/2})TiO_3$-$Ba(Al_{1/2}Nb_{1/2})TiO_3$ Solid Solution Ceramics". *Jap. J. Appl. Phys*. 48 , 09KC08-1-4 (2009).
[51] M.S. Yoon,Y.G. Lee and S.C.Ur. "Effects of co-doped CaO/MnO on the piezoelectric/ dielectric properties and phase transition of lead-Free $(Bi_{0.5}Na_{0.5})_{0.94}Ba_{0.06}TiO_3$ piezoelectric ceramics". *J Electroceram.* 23 564-571 (2009).
[52] M.S. Yoon, N. H. Khansur, S.C. Ur. "The effect of pre-milling/pre-synthesis process and excess Ba on the microstructure and dilectric/piezoelectric properties of nano-sized $0.94[(Bi_{0.5}Na_{0.5})TiO_3]$- $0.06[BaTiO_3]$". *Ceram.Intl.* 36 , 1265-1275 (2010).
[53] X.X. Wang, H.L.W. Chan, C.L. Choy, "$(Bi_{0.5}Na_{0.5})_{0.94}Ba_{0.06}TiO_3$ lead-free ceramics with simultaneous addition of CeO_2 and La_2O_3". *Appl. Phys. A –Mater. Sci.Process* 80 , 333-336 (2005).
[54] S. Greicius, J. Banys, R. Zhuo and T. Granzow "Dielectric investigations of $0.945(Bi_{0.5}Na_{0.5})TiO3$-0.055BaTiO3". *IEEE Trans. Ultrasonics Ferroelectric and Frequency Control* 56(9), 1831-1834 (2009).
[55] J.R. Gomah-Pettry, S. Said, P. Marchet anf , J.P. Mercurio."Sodium-bismuth titanate based lead-free ferroelectric materials". *J. Eur. Ceram. Soc*. 24 , 1165–116 (2004).
[56] G. Xu, D.Yang, K.Chen, D.A. Payne and J. F. Carroll III. "Growth, domain dynamics and piezoelectric properties of some lead-free ferroelectric crystals". *J Electroceram*. 24 , 226-230 (2010).
[57] R. Ahluwalia, T. Lookman, A. Saxena and W. Cao. "Domain size dependence of piezoelectric properties in ferroelectrics". *Phys.Rev.B* 72 , 014112-1-13 (2005).

Figure captions

Figure 1. Selected peaks of the XRD patterns of poled BNBT6-1 to 3 ceramics: (a) Evolution with the poling degree of the (006) and (202)-rhombohedral doublet and the (111)-tetragonal peak; (b) Evolution with the poling degree of the (024)-rhombohedral peak and the (002) and (200)-tetragonal doublet.

Figure 2. SEM micrographs of polished and etched surfaces of the BNBT6-1 to 3 ceramics.

Figure 3. Resonance spectra of BNBT6-3 ceramic: (a) planar and (b) thickness resonance modes of a thickness poled an excited thin disk; shear mode of thickness-poled and length-excited rectangular plate, (c) coupled with other plate modes and (d) decoupled by fine-tuning of the thickness. Experimental spectra (symbols) and reconstructed ones (lines) after calculation of coefficients by Alemany et al. software are shown for all resonances together with the values of the regression factor (R^2).

Figure 4. Dielectric permittivity, real part and losses, of poled BNBT6-1 to 3 ceramics measured on heating. Arrows indicate the increasing measurement frequency (1, 2, 5, 10, 50, 100, 200, 500 and 1000 kHz) and critical temperatures commented in the text.

Figure 5. Dielectric permittivity, real part and losses, of thermally depoled BNBT6-1 to 3 ceramics measured on cooling. Arrows indicate the increasing measurement frequency (1, 2, 5, 10, 50, 100, 200, 500 and 1000 kHz) and critical temperatures commented in the text.

Figure 6. (a) Shear mode resonance spectra of thickness-poled and length-excited plate of BNBT6-3 ceramic at 140ºC. Experimental spectra (symbols) and reconstructed ones (lines) after calculation of coefficients by Alemany et al. software are shown together with the value of the regression factor (R^2). (b) The thermal evolution of the thickness resonance of a thickness-poled and excited disk of BNBT6-3 ceramic and the thermal evolution of the radial mode of coarse grained BNBT6 from [46].

Table captions

Table 1. Relative density, parameters from the quantitative characterization of grain (SEM) and pore (Optical Microscopy=OM) size, as well as the total porosity, together with the piezoelectric, elastic and dielectric parameters, as well as electromechanical coupling factors and frequency numbers, obtained from the uncoupled shear resonances of, thickness-poled and longitudinally excited, plates of BNBT6 ceramics. Data from the literature are also shown for comparison.

Table 2. Relative density, mean grain size, and piezoelectric, elastic and dielectric parameters, as well as electromechanical coupling factors and frequency numbers, obtained from planar (P) and thickness (T) resonances of thin ceramics disk of BNBT6 ceramics, poled and excited in thickness. Data from the literature are also shown for comparison.

Table 1

Composition, Synthesis route, Processing conditions	BNBT6 sol-gel autocombustion HP + recrystallization			BNBT6 [22] mixed oxides sintering 1200ºC 2h	BNT [15] mixed oxides sintering 1100ºC 2h
	BNBT6-1 HP700ºC/2h+ 1000ºC-1h	BNBT6-2 HP800ºC/2h+ 1000ºC-1h	**BNBT6-3 HP800ºC/2h+ 1050ºC-1h**		
Relative density (%)	82.9	94.5	**95.4**	98.3	---
Number of grains SEM	340	530	**473**	---	---
<G> (nm) SEM	(720±20)	(580±10)	**(680 ± 10)**	>1000	>1000
σ_G (nm) SEM	(660±40)	(470±10)	**(500 ± 20)**	---	---
Number of pores OM	793	1476	**792**	---	---
<P> (μm) OM	(0,95 ± 0,02)	(2,08 ± 0,01)	**(2,13 ± 0,01)**	---	---
σ_p (μm) OM	(0,60 ± 0,01)	(0,40 ± 0,01)	**(0,31 ± 0,01)**	---	---
P (%) OM	20,4	3,24	**2,0**	---	---
Number of grains SEM	351	482	**473**	---	---
R^2	0.8828	0.9818	**0.9847**	NA	NA
K_{15}(%)	11.0	36.6	**40.2**	49.8	36.2
N_{15}(kHz.mm)	1300	1365	**1373**	1568	1650
ε^S_{11}	806 – 72i	600 - 33i	**609 - 29i**	---	---
ε^σ_{11}	816 - 75i	692 - 43i	**726 - 40i**	373 (1KHz)	367(1MHz)
e_{15} ($C.m^2$)	1.70-0.23i	5.87 –0.25i	**6.55 – 0.23i**	---	---
d_{15} (10^{-12} $C.N^{-1}$)	50.7 - 8.3i	140.1 - 8.9i	**158.3 – 8.31i**	194	87.3
h_{15} (10^8 $V.m^{-1}$)	2.39 - 0.10i	11.04 +0.13i	**12.16 + 0.16i**	---	---
g_{15} (10^{-3} $m.V.N^{-1}$)	7.07 –0.50i	22.83 –0.05i	**24.64 + 0.05i**	---	---
s^E_{55} (10^{-12} m^2N^{-1})	29.9 - 0.93 i	23.87 – 0.51i	**24.17 - 0.42i**	23.3	17.9

Table 2

Composition, Synthesis route, Processing conditions		BNBT6 sol-gel autocombustion HP + recrystallization 1000-1050ºC/1h			BNBT6 [21] mixed oxides sintering 1200ºC/2h	BNBT6 [45] mixed oxides sintering 1160-1180ºC/1h	BNT[15] mixed oxides sintering 1100ºC/2h
		BNBT6-1 HP700ºC/2h+ 1000ºC-1h	BNBT6-2 HP800ºC/2h+ 1000ºC-1h	**BNBT6-3 HP800ºC/2h+ 1050ºC-1h**			
Relative density (%)		82.9	94.5	**95.4**	98.3	---	---
Mean grain size (nm)		720	580	**680**	> 1000	---	---
Berlincourt d_{33} (10^{-12}C.N^{-1})		105	143	**148**	125	122	72.9
R^2	P	0.9977	0.9997	**0.9999**	NA	NA	NA
R^2	T	0.9909	0.9736	**0.9548**	NA	NA	NA
k_p (%)	P	13.6	24.6	**26.8**	20	29	16.8
N_p(kHz.mm)	P	2535	2873	**2933**	3000	3000	3260
k_{31} (%)	P	8.2	14.8	**15.74**	19.2	---	10.2
k_t (%)	T	29.5	36.4	**40.4**	52	40	45.5
N_t(kHz.mm)	T	1855	2238	**2281**	2600	2522	2780
$\varepsilon^{\sigma}_{33}$	P	465-24i	636 – 34i	**641 – 31i**	580 (1KHz)	601 (1KHz)	343 (1MHz)
tan δ ($\varepsilon^{\sigma}_{33}$)	P	0.052	0.054	**0.048**	0.013 (1KHz)	0.018 (1KHz)	0.028 (1MHz)
ε^{S}_{33}	T	391 – 16 i	476 – 33 i	**456-31 i**	---	---	---
h_{33}(10^8 V/m)	T	13.6 + 0.37 i	19. 9 +0.34 i	**23.4 - 0.07 i**	---	---	---
e_{33} (C.m^2)	T	4.70 –0.06i	8.38-0.43i	**9.46-0.67i**	---	---	---
d_{31} (10^{-12} C.N^{-1})	P	-19.9+0.97i	-34.8 + 1.37i	**-37.0 + 1.33i**	- 40	---	-15.0
g_{31}(10^{-3} m.V.N^{-1})	P	-4.84 - 0.01i	-6.17 –0.08i	**-6.51 –0.08i**	---	---	---
c^{D}_{33} (10^{10} N.m^2)	T	7.28+0.60 i	12.61+0.30i	**13.62 +0.45i**	---	---	---
Poisson ratio	P	0.27	0.27	**0.31**	---	0.25	0.263
s^{E}_{11} (10^{-12} m^{2}N^{-1})	P	14.30 - 0.20 i	9.57 - 0.09i	**9.73 – 0.07i**	8.59	---	7.07
s^{E}_{12} (10^{-12} m^{2}N^{-1})	P	-3.89 + 0.05 i	-2.90 + 0.03i	**-3.02 + 0.02i**	---	---	---
s^{E}_{66} (10^{-12} m^{2}N^{-1})	P	36.36 – 0.49i	24.94 – 0.23i	**25.52-0.19i**	---	---	---

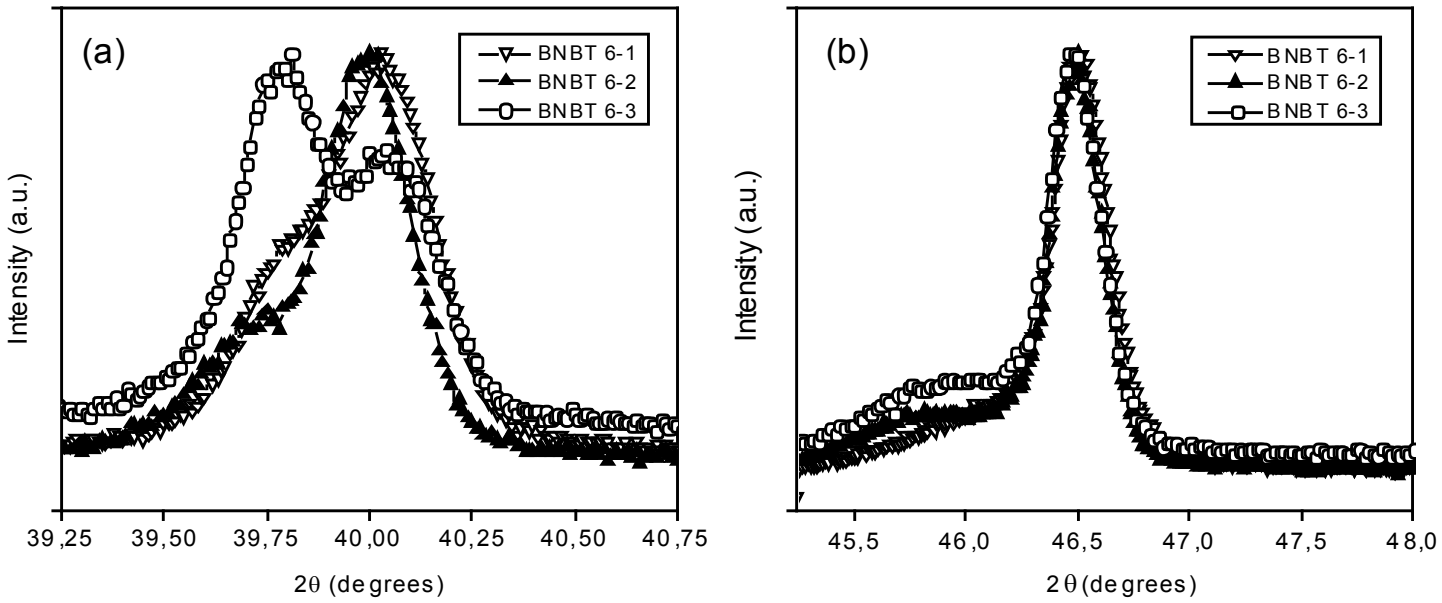
(a)
BNBT 6-1
BNBT 6-2
BNBT 6-3
Intensity (a.u.)
39,25
39,50
39,75
40,00
40,25
40,50
40,75
2θ (degrees)
(b)
BNBT 6-1
BNBT 6-2
BNBT 6-3
Intensity (a.u.)
45,5
46,0
46,5
47,0
47,5
48,0
2θ (degrees)

Fig.1.

BNBT6-1 (HP700ºC-2h+1000ºC-1h)

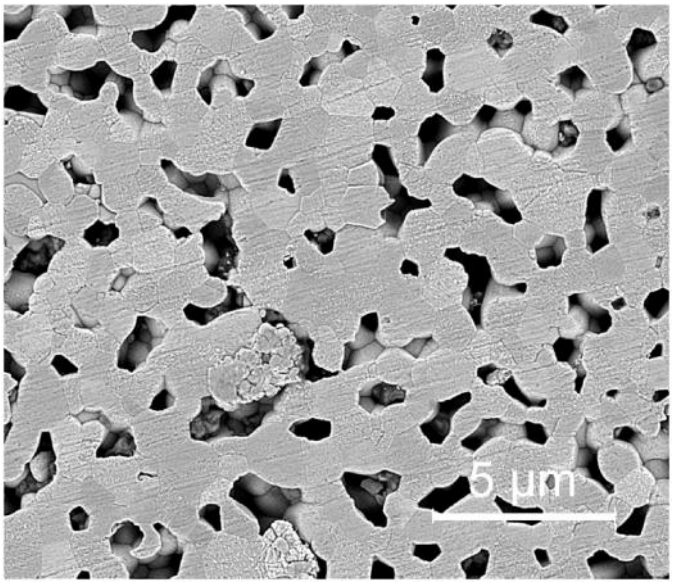

BNBT6-2 (HP800ºC-2h+1000ºC-1h)

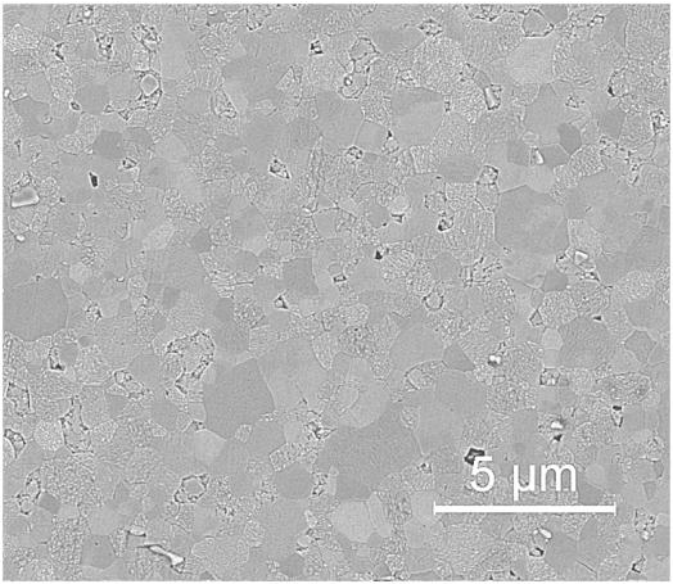

BNBT6-3 (HP800ºC-2h+1050ºC-1h)

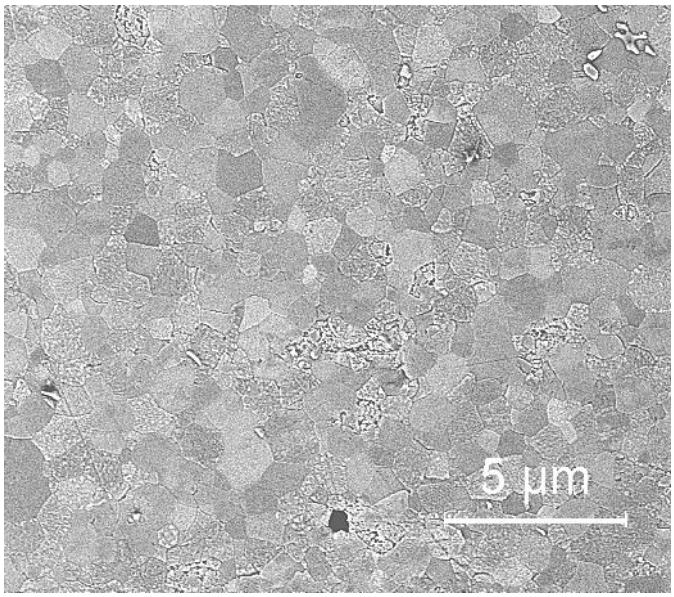

Fig.2.

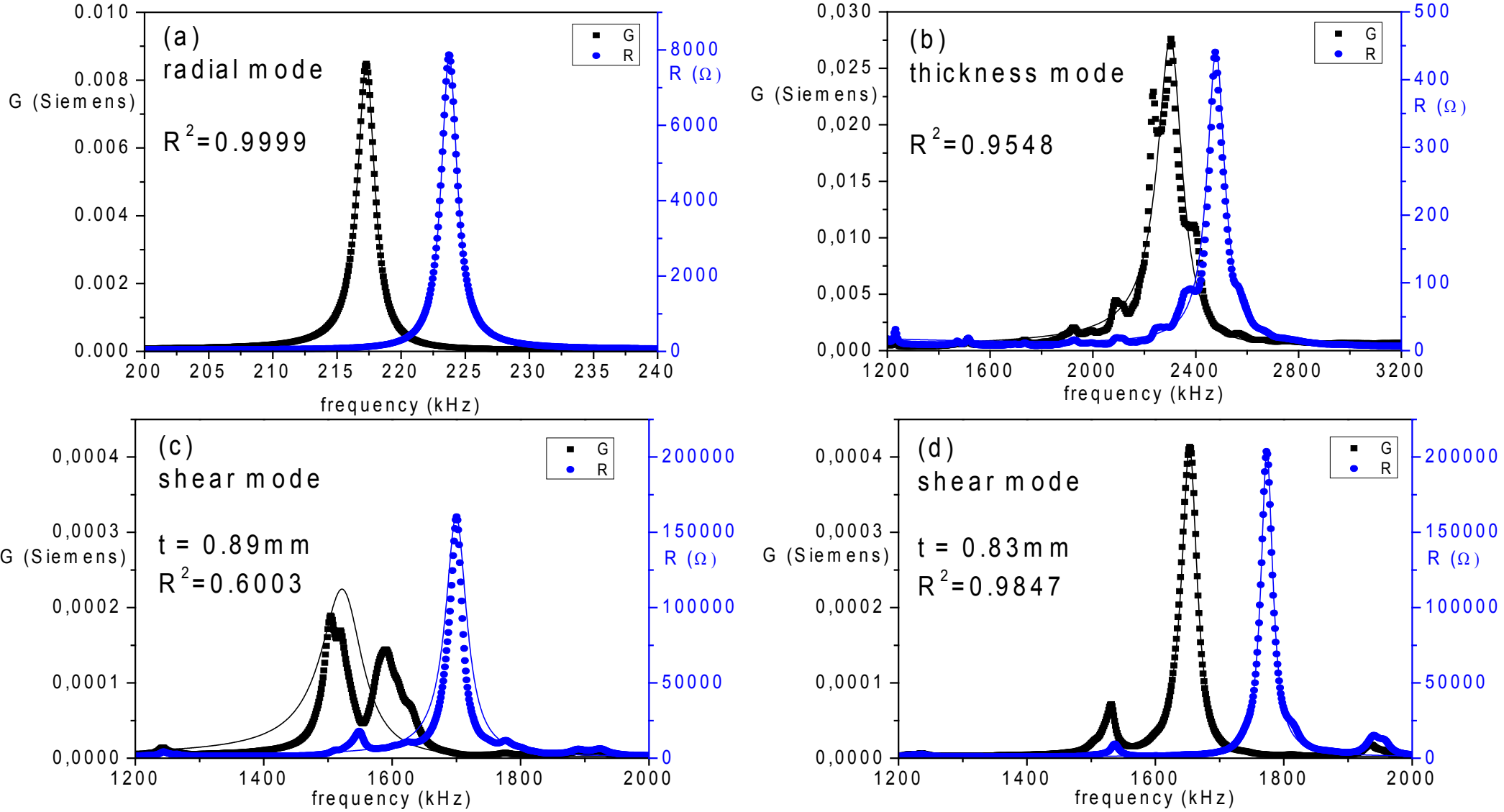
(a)
radial mode
R²=0.9999
G
R
G (Siemens)
R (Ω)
frequency (kHz)
(b)
thickness mode
R²=0.9548
(c)
shear mode
t = 0.89mm
R²=0.6003
(d)
shear mode
t = 0.83mm
R²=0.9847

Fig. 3

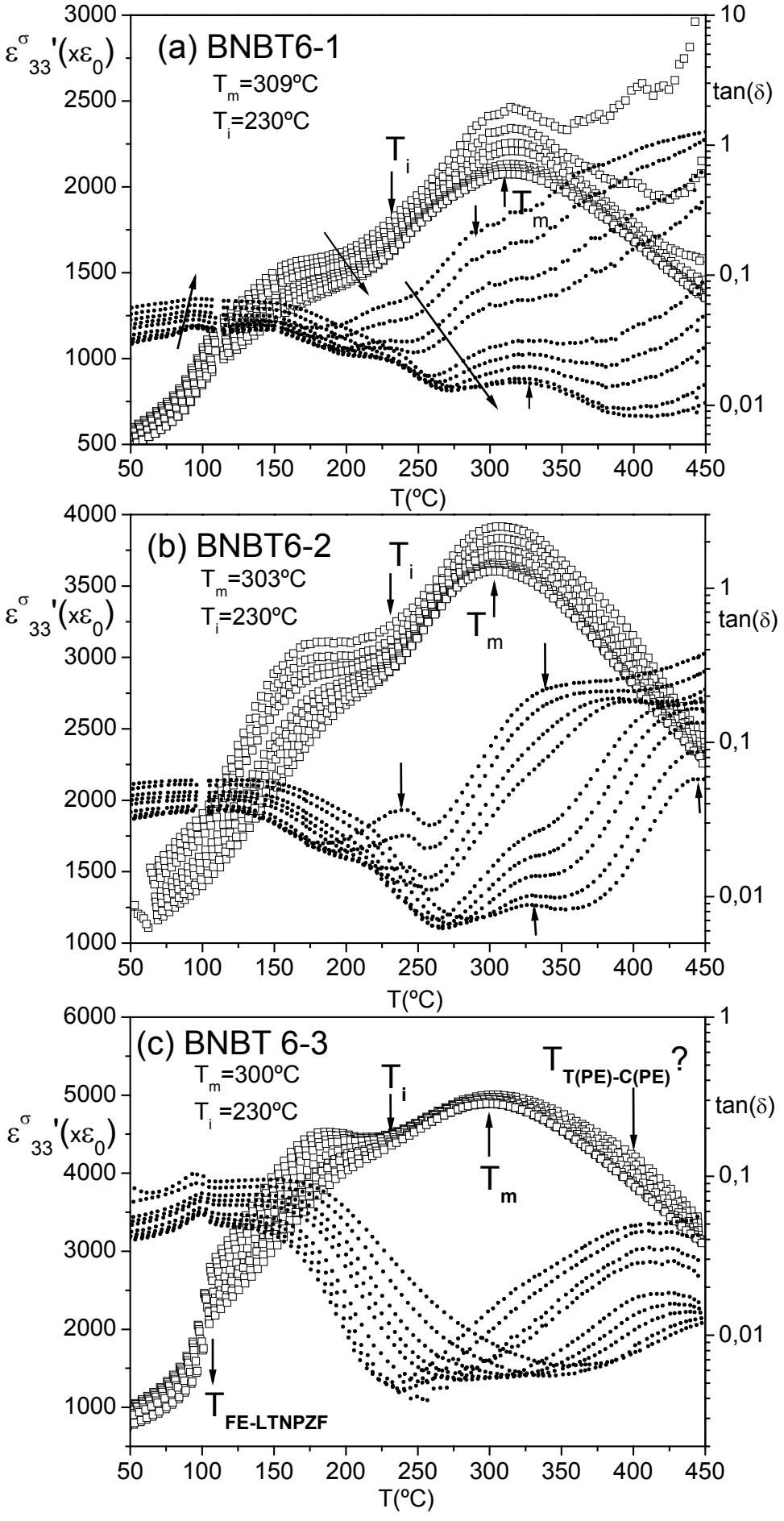
(a) BNBT6-1
T_m=309ºC
T_i=230ºC
T_i
T_m
$\varepsilon^{\sigma}_{33}'(x\varepsilon_0)$
tan(δ)
T(ºC)
(b) BNBT6-2
T_m=303ºC
T_i=230ºC
T_i
T_m
$\varepsilon^{\sigma}_{33}'(x\varepsilon_0)$
tan(δ)
T(ºC)
(c) BNBT 6-3
T_m=300ºC
T_i =230ºC
T_i
T_m
$T_{T(PE)-C(PE)}$?
$T_{FE-LTNPZF}$
$\varepsilon^{\sigma}_{33}'(x\varepsilon_0)$
tan(δ)
T(ºC)

Fig. 4

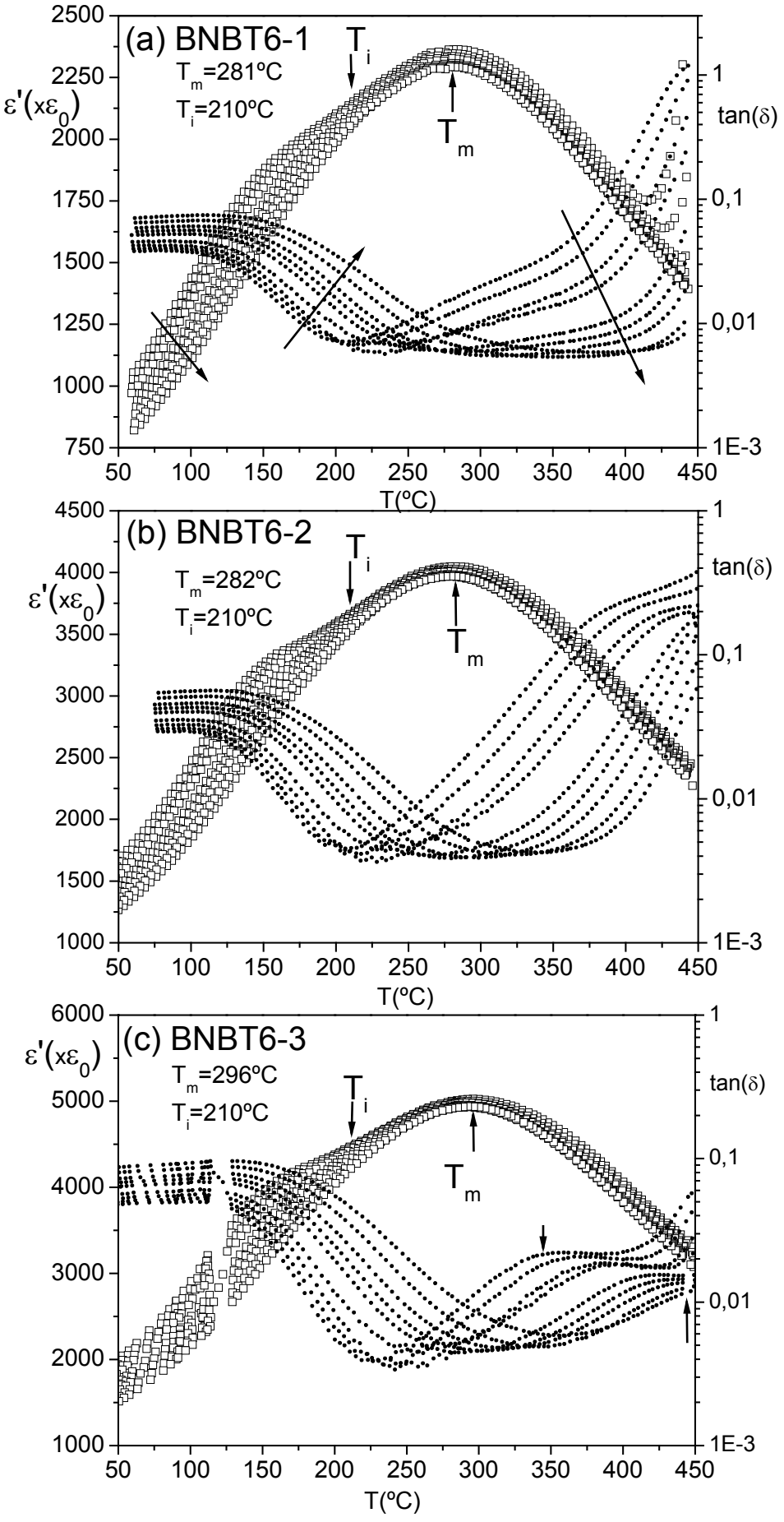
(a) BNBT6-1
T_m=281ºC
T_i=210ºC
T_i
T_m
ε'(xε_0)
tan(δ)
T(ºC)
(b) BNBT6-2
T_m=282ºC
T_i=210ºC
(c) BNBT6-3
T_m=296ºC
T_i=210ºC

Fig. 5

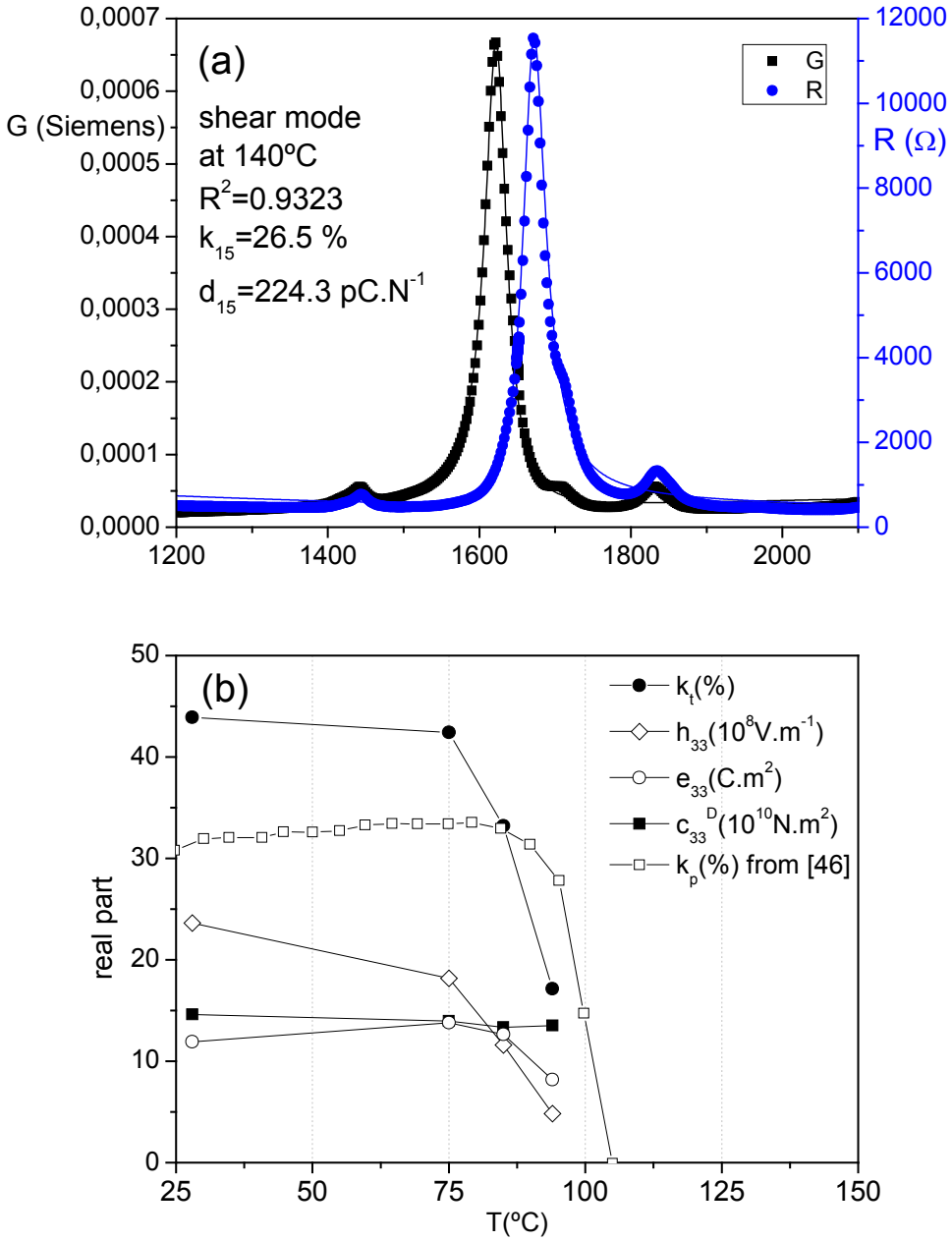
(a)
shear mode
at 140ºC
R²=0.9323
k15=26.5 %
d15=224.3 pC.N-1
G
R
G (Siemens)
R (Ω)
0,0007
0,0006
0,0005
0,0004
0,0003
0,0002
0,0001
0,0000
12000
10000
8000
6000
4000
2000
0
1200
1400
1600
1800
2000
(b)
kt(%)
h33(10⁸V.m-1)
e33(C.m²)
c33D(10¹⁰N.m²)
kp(%) from [46]
real part
T(ºC)
50
40
30
20
10
0
25
50
75
100
125
150

Fig.6